Available online at www.sciencedirect.com

ScienceDirect

Ceramics International 39 (2013) 8715–8722

CERAMICS INTERNATIONAL

www.elsevier.com/locate/ceramint

Green sonochemical synthesis of cupric and cuprous oxides nanoparticles and their optical properties

Anze Shui*, Wenli Zhu, Linfeng Xu, Dong Qin, Yanmin Wang

College of Materials Science and Engineering, South China University of Technology, Guangzhou 510641, China

Received 18 December 2012; received in revised form 12 April 2013; accepted 16 April 2013
Available online 27 April 2013

Abstract

Nanoparticles of cupric oxide (CuO) and cuprous oxide (Cu_2O) with various morphologies were synthesized by a green sonochemical process without any surfactants and templates. The Cu_2O nanoparticles with the truncated cubic, cubic octahedral and octahedral morphologies were prepared via the deoxidation of the CuO nanoparticles. The Cu_2O and CuO samples were characterized by X-ray diffraction (XRD), scanning electron microscopy (SEM), and ultraviolet visible absorption spectroscopy (UV–vis). The experimental results indicate that the molar ratio of sodium hydroxide to copper sulfate affects the morphology and size of the CuO and Cu_2O nanoparticles produced by the sonication. The band gap energy of CuO nanoparticles was 1.45–1.75 eV, the morphology had a great effect on the optical properties of CuO. The Cu_2O nanoparticles had broad emission peaks at the visible region, and the band gap energy was estimated to be 1.95–2.09 eV. The growth mechanisms of the CuO and Cu_2O nanoparticles are discussed.
Published by Elsevier Ltd and Techna Group S.r.l.

Keywords: Cupric oxide; Cuprous oxide; Nanoparticle; Sonochemical synthesis

1. Introduction

Various nano-materials such as nanowire [1], nanoribbon [2], nanorod [3], nanosheet [4], nanoring [5], nanobelt [6], nanoflower [7], microsphere [8], by-pyramid [9], and cage [10] have attracted much attention due to their unique optical, electrical, magnetic properties and the potential applications in various nanodevices [11].

CuO and Cu_2O are typical transition metal oxide semiconductors of p-type in the bandgap range 1.8–2.5 eV and 1.2–2.0 eV [12] as promising materials in various applications such as lithium battery [13–15], gas sensor [16], catalyst [17], photoelectrochemical material [18], solar energy system [19], biosensor [20], and photocatalyst [21]. The CuO nanoflat is a particulate material in pigment and coating applications, compared to the other powders with various morphologies, due to its good adhesive ability, shielding effect, light-reflecting ability and dispersion property [15]. Also, there are three main advantages for Cu_2O nanoparticle as a photocatalyst, i.e., (i) it is low toxic and inexpensive [22], (ii) it can effectively utilize the visible light [23], and (iii) it can powerfully adsorb the molecular oxygen [24,25], which scavenges photoelectron to constrain the combination of electron and hole. Zhu et al. [26] reported that spherical and octahedral Cu_2O nanoparticles can decompose the rhodamine B 55.68% and 41.16%, respectively.

Since the chemical and physical properties of CuO and Cu_2O nanoparticles strongly depend on their microstructures such as the orientation, grain size and morphology [27], CuO and Cu_2O nanoparticles with various morphologies have been synthesized over the past decades. Some synthesis techniques are developed to control the microstructures, which include the chemical vapor deposition method [28], the hydrothermal method [29], the solution synthesis method [30] and the electrodeposition technique [31]. However, there are a few papers to report the sonochemical synthesis of the CuO and Cu_2O nanoparticles, especially green sonochemical synthesis technique without any surfactants and templates.

The sonochemical synthesis technique is a promising method for the preparation of various nano-materials such as metal, oxide, sulfide and carbide [32]. This technique uses the acoustic cavitation phenomenon for the synthesis due to the

*Corresponding author. Tel.: +86 20 87110290; fax: +86 20 87110273.
E-mail address: shuianze@scut.edu.cn (A. Shui).

0272-8842/$ - see front matter Published by Elsevier Ltd and Techna Group S.r.l.
http://dx.doi.org/10.1016/j.ceramint.2013.04.055

continuous formation, growth and drastic collapse of bubbles in solution. When the container with the solution is put in an ultrasound reactor, high temperature (> 5000 K), high pressure (> 20 MPa) and high cooling rate (10^{10} K s^{-1}) are generated in the collapse of bubbles, accompanying with the intense shock wave and micro-jet (400 km/h) [33,34]. These behaviors can prevent the nuclear growth and the secondary nucleation. The sonochemical technique is more convenient, economical, effective and environment friendly rather than the other techniques [35]. Deng et al. [36] synthesized the hierarchical CuO hollow submicron-sized spheres by the sonochemical technique with urea as alkali and the decomposition of CO_2 as a template.

In this paper, the CuO nanoparticles with various morphologies were synthesized by a green sonochemical technique with copper sulfate pentahydrate and sodium hydroxide as raw materials, without any surfactants and templates. The truncated cubic, cubic octahedral and octahedral Cu_2O nanoparticles were prepared via the deoxidation of the CuO nanoparticles. In addition, the morphology evolution of the CuO and Cu_2O nanoparticles were also discussed.

2. Experimental

Analytical grade of reagents were used as raw materials. The experimental conditions were optimized according to the various pre-experiment results. In a typical CuO synthesis process, aqueous solution of $CuSO_4 \cdot 5H_2O$ (0.1 M) was added into aqueous solution of sodium hydroxide (0.05 M) in a beaker, and stirred for 10 min to make the homogeneous precursor solution. The beaker was covered with a polyethylene film, and transferred into an ultrasonic bath (KQ50-DE, Kunshan ultrasonic instrument Co. Ltd., China) without stirring at 80 °C for 30 min. The reaction mixture was aged at 25 °C for 12 h. The obtained black precipitate was filtered by microporous membrane with the pore size of 0.45 μm, and washed for several times with deionized water and anhydrous ethanol. The black CuO products were obtained after drying at 60 °C for 12 h.

In the Cu_2O synthesis process, the solution pH was adjusted with ammonia, while the above sonication reaction without stirring at 80 °C for 10 min, the beaker was shifted out from the ultrasonic bath, and aqueous solution of ascorbic acid (0.1 M) was added into the beaker with stirring for 10 min. Then the beaker was reput into the ultrasonic bath without stirring at 80 °C for 20 min. The orange Cu_2O products were finally obtained after the same post-treatment.

The CuO and Cu_2O samples were characterized by X-ray diffraction (XRD, Philips PW-1710 model X-ray diffractometer, the Netherlands) using Cu K_α, scanning electron microscope (SEM, Nova NanoSEM 430, the Netherlands) and UV/visible/near infrared spectrophotometer (LAMBDA950, U.S.A). The solution pH value was determined by a pH meter (PHS-3C, Shenzhen Dingxin Equipment Co. Ltd., China).

3. Results and discussions

Fig. 1 shows the microstructures and optical property of the CuO sample prepared at the molar ratio of sodium hydroxide to copper sulfate (marked as M) of 2.5. Fig. 1(a) is the SEM image of the CuO sample. The CuO nanoparticles exhibit

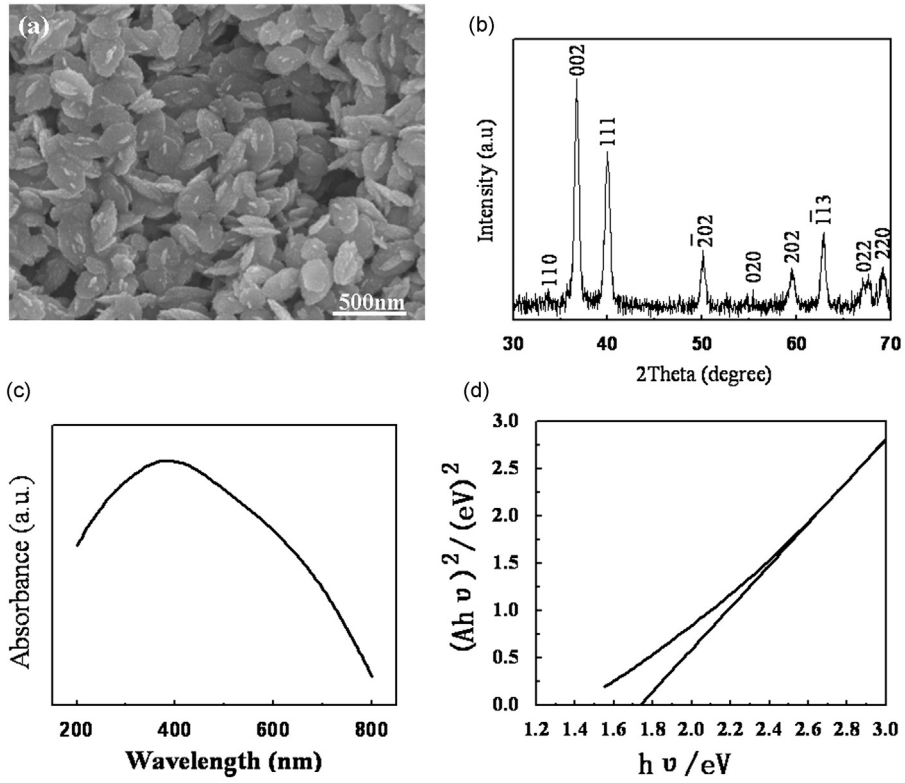

Fig. 1. (a) SEM image, (b) XRD pattern, (c) UV–vis absorption spectrum and (d) $(Ah\upsilon)^2$–$h\upsilon$ curves of the CuO sample prepared at *M* 2.5.

spindle-like structure and the size was estimated to be 300 nm and 170 nm. Fig. 1(b) is the XRD pattern of the CuO sample. All peaks in the pattern were assigned to the CuO monoclinic phase with lattice constants $a=0.4686$, $b=0.3432$ and $c=0.5128$ nm, which were in good agreement with the standard data form (JCPDS 05-0661, space group $C_{2/C}$). To examine the optical property of the spindle-like CuO nanoparticles, the optical absorption experiment was carried out by a UV/visible/near infrared spectrophotometer. A broad absorption peak at ~375 nm in the UV region was observed as shown in Fig. 1(c). Fig. 1(d) shows the $(Ahv)^2$–hv curves of the spindle-like CuO nanoparticles, there was a linear relationship between $(Ahv)^2$ and hv in the range of 2.45 to 3.00 eV. The band gap of the spindle-like CuO nanoparticles was estimated to be 1.74 eV, according to the prolongation of linear section. Compared to the bulk CuO (1.2 eV), the blue shift phenomenon can be attributed to the quantum size effect [37].

In order to compare the effect of sonication, at M 2.5, CuO samples were not treated by the sonication under the same reaction conditions and post-treatments, the morphology of the samples changed as shown in Fig. 2(b). The particle size is nonuniform, and part of the CuO particles display spindle-like, but most of the particles aggregate together, compared with the CuO samples with the sonication treatment as shown in Fig. 2(a).

To examine the formation mechanism of the CuO spindle-like structure, a series of contrast experiments were carried out at various M values under the same other conditions. Fig. 3 shows the SEM images of the CuO samples prepared at M 2.0, 3.0, 4.0 and 5.0, respectively. At M 2.0, the spindle-like and

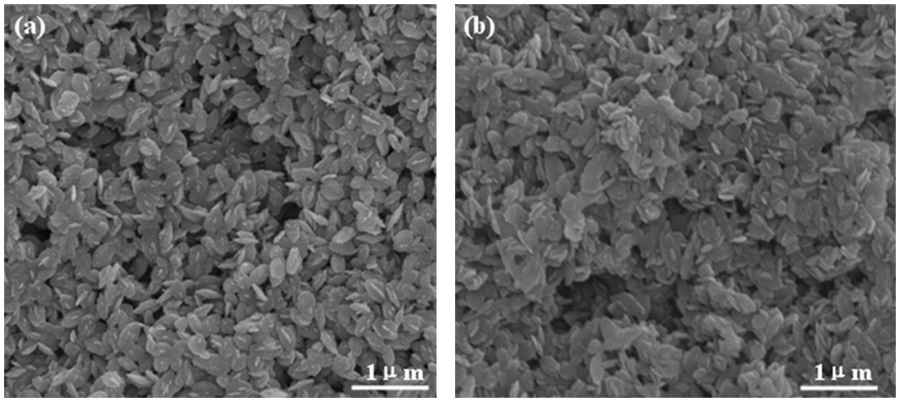

Fig. 2. SEM images of the CuO samples for M 2.5 treated (a) with sonication and (b) without sonication.

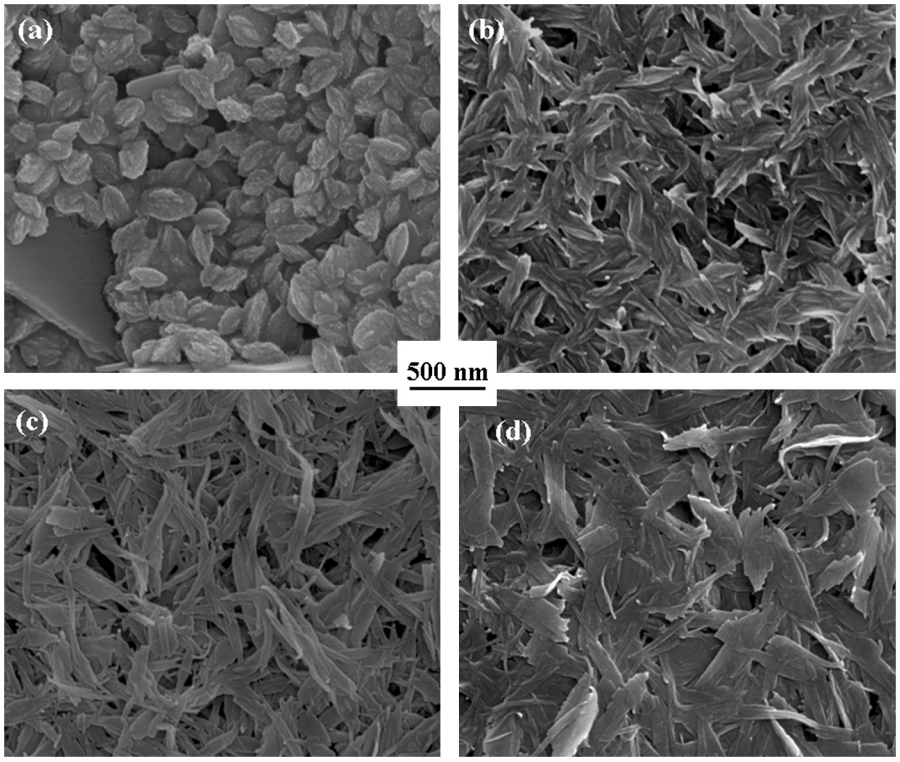

Fig. 3. SEM images of the CuO samples prepared at M (a) 2.0, (b) 3.0, (c) 4.0, and (d) 5.0, respectively.

flat structures are observed. At *M* 3.0, the long diameter of the nanospindle increases to display nanorod with the diameter and length of approximately 70 nm and 350 nm, respectively. At *M* 4.0, however, the structure displays the nanoribbon with the longer length. At *M* 5.0, the structure presents irregular flat. The results indicate that the size and morphology of the CuO nanoparticles significantly depend on the molar ratio of sodium hydroxide to copper sulfate.

Fig. 4 shows the XRD patterns of the CuO samples prepared at *M* 2.0, 3.0, 4.0 and 5.0, respectively, all peaks can be indexed as a monoclinic CuO phase (JCPDS 05-0661, space group $C_{2/C}$). There is no significant change in the XRD patterns.

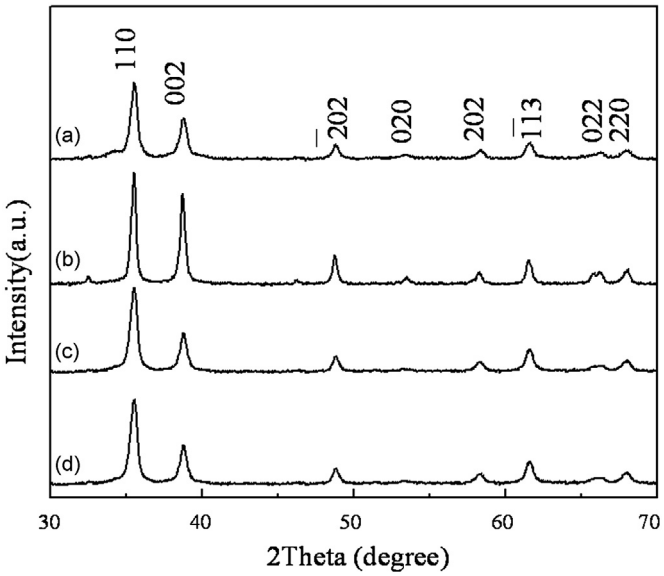

Fig. 4. XRD patterns of the CuO nanoparticles prepared at *M* (a) 2.0, (b) 3.0, (c) 4.0, and (d) 5.0.

Based on these results, the formation mechanism of the CuO structure is proposed, the main chemical reactions can be expressed as follows:

$$CuSO_4+6H_2O \rightarrow [Cu(H_2O)_6]^{2+}+SO_4^{2-} \quad (1)$$

$$NaOH \rightarrow Na^+ + OH^- \quad (2)$$

$$[Cu(H_2O)_6]^{2+}+2OH^- \rightarrow Cu(H_2O)_4(OH)_2+6H_2O \quad (3)$$

$$Cu(H_2O)_4(OH)_2 \rightarrow CuO+5H_2O \quad (4)$$

In the reaction system, $CuSO_4$ dissociates to release Cu^{2+}, and exists as $[Cu(H_2O)_6]^{2+}$ in the aqueous solution [Eq. (1)], then the $[Cu(H_2O)_6]^{2+}$ coordinates with OH^-, which is derived from the hydrolyzation of NaOH to form $Cu(H_2O)_4(OH)_2$, [Eqs. (2) and (3)]. The newly-produced $Cu(H_2O)_4(OH)_2$ dehydrolyzes to generate CuO monomers in the alkaline solution under ultrasonic radiation [Eq. (4)]. The primary CuO monomers aggregate under the acoustic cavitation, it can be deemed to be the process of oriented aggregation. As the nanocrystals grow along (002) plane, the spindle-like CuO nanostructures are formed [38]. The CuO nanocrystals still grow preferentially along (002) plane when the sodium hydroxide concentration (i.e. the *M* value) increases, resulting in the generation of nanorod and nanoribbon. However, the CuO nanocrystals aggregate randomly when the *M* is greater than 4.0. Fig. 5 shows the schematic diagram of the formation of the CuO nanoparticles.

UV–vis absorption spectra of CuO nanoparticles in aqueous solution is shown in Fig. 6(a)–(d), and Fig. 6 (e)–(f) shows the curves of $(Ahv)^2$ versus hv for a direct transition of Fig. 6(a)–(d). The wavelengths of peak and the band gaps of the CuO samples are summarized in Table 1. The results indicate that the optical band gaps can be fine-tuned in 1.45–1.75 eV. The highest band gap is 1.75 eV when $M=3.0$, which is much wider than the bulk CuO (1.2 eV).

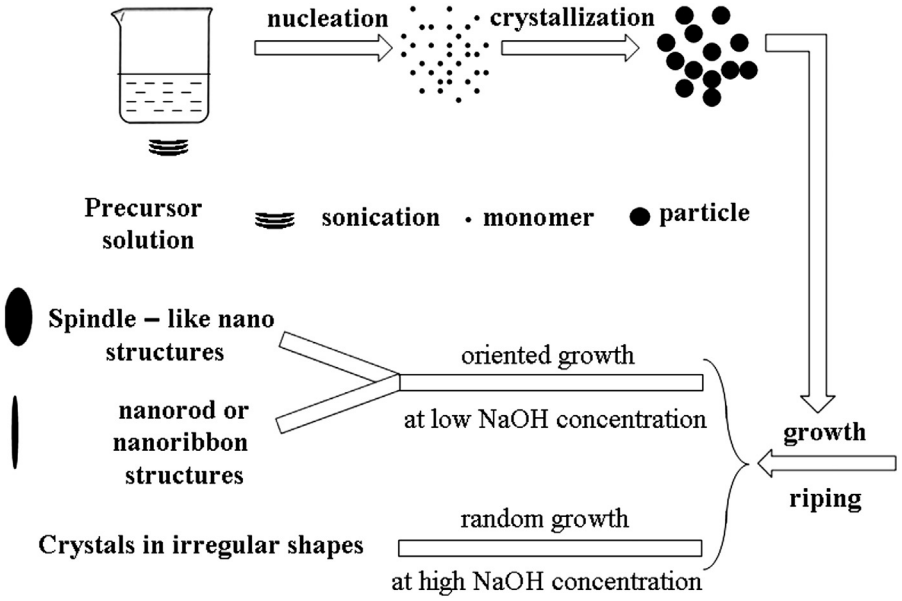

Fig. 5. Schematic diagram of the formation of the CuO nanoparticles.

Fig. 7 shows the SEM images of the Cu_2O and CuO samples prepared at *M* 2.5, *M* 3.0, and *M* 4.0 and pH 11.7, 12.9, and 13.1, respectively. When $M=2.5$, and pH = 11.7, the CuO are mainly consisted of nanoribbon with some irregular flat, the corresponding Cu_2O with the size of 250–500 nm is of truncated cubic morphology. On the other hand, the CuO nanoparticles mainly display irregular flat with some nanorod when the *M* value increases, and the morphology of Cu_2O changes from truncated cubic to cuboctahedron. When $M=4.0$, and pH = 13.1, the CuO is completely irregular flat,

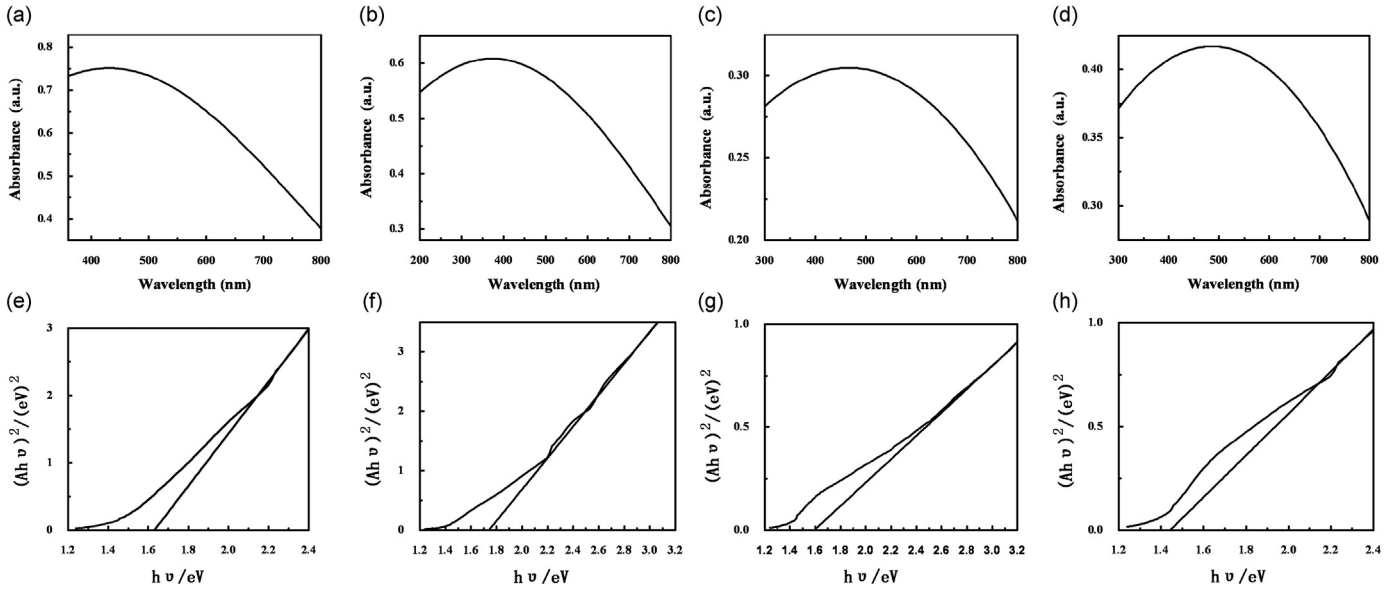

Fig. 6. UV–vis absorption spectra ((a), (b), (c),(d)) and $(Ahv)^2$–hv curves ((e), (f), (g),(h)) of the Cu_2O samples ((a),(e) for *M* 2.0, (b), (f) for *M* 3.0, (c), (g) for *M* 4.0, (d), (h) for *M* 5.0).

Table 1
The wavelength of the peak and the band gap of the CuO samples.

M value	The wavelength of the peak (nm)	The band gap (eV)
2.0	431	1.63
3.0	370	1.75
4.0	465	1.60
5.0	500	1.45

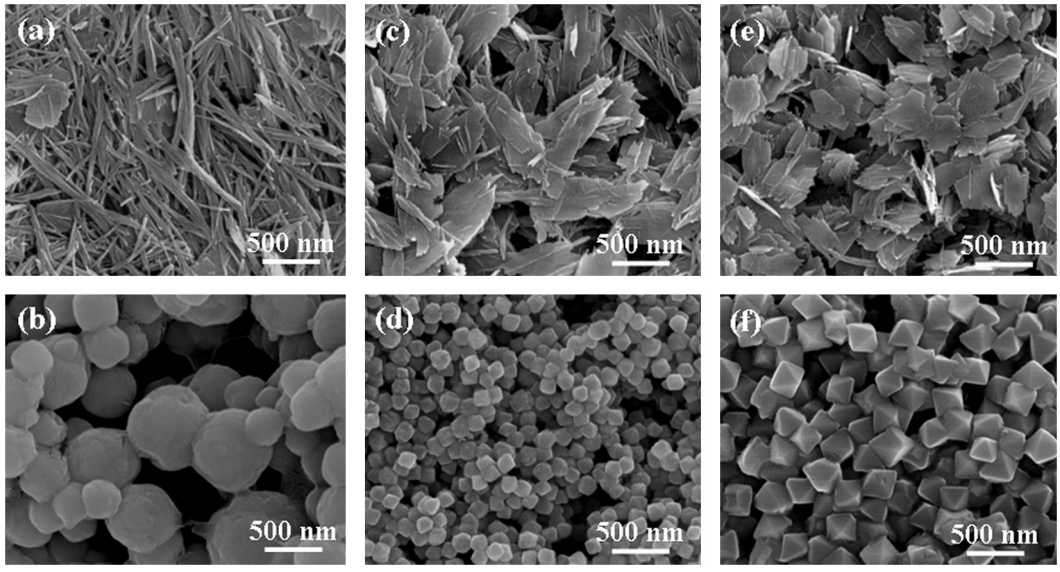

Fig. 7. SEM images of the CuO and Cu_2O samples prepared at $M=2.5$, pH = 11.7 for (a) and (b), $M=3.0$, pH = 12.9 for (c) and (d), $M=4.0$, pH = 13.1 for (e) and (f), respectively.

as shown in Fig. 7(e), and the corresponding Cu_2O presents uniform octahedron, and the edge length is 170 nm as shown in Fig. 7(f). These results indicate that the sodium hydroxide concentration (i.e. *M*) has an effect on the morphology and size of CuO and Cu_2O nanoparticles synthesized.

Fig. 8(a)–(c) shows the XRD patterns of the truncated cubic, cubic octahedral and octahedral Cu_2O nanoparticles, respectively. Six characteristic peaks for (110), (111), (200), (220), (311) and (222) planes were observed at 2θ 29.6°, 36.5°, 42.4°, 61.5°, 73.7° and 77.6°, respectively, which were in good agreement with the standard data form (JCPDS 05-0667, space group Pn3m, $a=4.4267$ Å). No peaks from other materials such as CuO and Cu can be observed, indicating the high purity of the samples. There is no significant change in the XRD patterns.

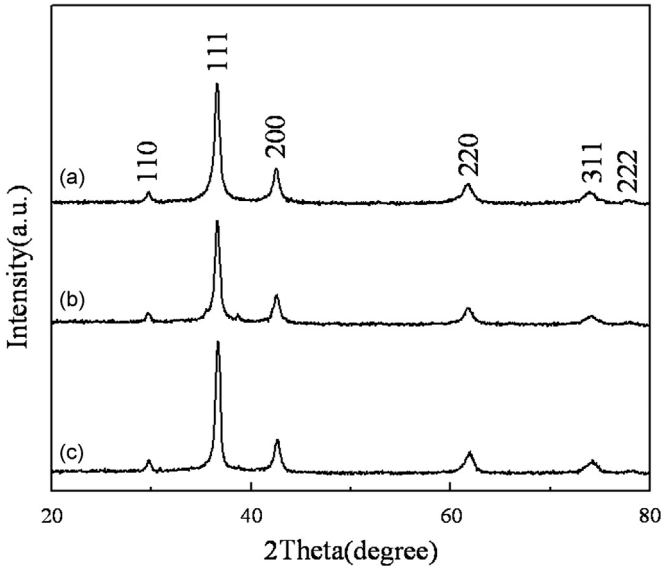

Fig. 8. XRD patterns of the Cu_2O nanoparticles ((a) truncated cube, (b) cuboctahedron, and (c) octahedron).

Fig. 9(a)–(c) are the UV–vis absorption spectra of the Cu_2O samples with different morphologies ((a) truncated cube, (b) cuboctahedron and (c) octahedron). The characteristic absorption peaks due to the surface-plasmon resonance (SPR) of Cu_2O colloids [39] are observed at about 430 nm, 480 nm, and 470 nm, respectively. The results indicate that the Cu_2O nanoparticles are sensitive to the visible light owing to the conductivity of Cu_2O powder. Fig. 9(d)–(f) shows the $(Ahv)^2$ versus hv curves for the truncated cubic, cubic octahedral and octahedral Cu_2O nanoparticles, respectively. The band gap of the Cu_2O nanoparticles is about 1.92–2.09 eV, indicating the obvious red shift, compared with that of bulk Cu_2O (2.17 eV) [40]. This is because the optical absorption is affected by the morphology and crystallinity of Cu_2O [41]. The wavelengths of peak and the band gaps of the Cu_2O samples are summarized in Table 2.

Table 2
The wavelength of the peak and the band gap of the Cu_2O samples.

Cu_2O	The wavelength of the peak (nm)	The band gap (eV)
Truncated cube	430	1.95
Cuboctahedron	480	1.92
Octahedron	470	2.09

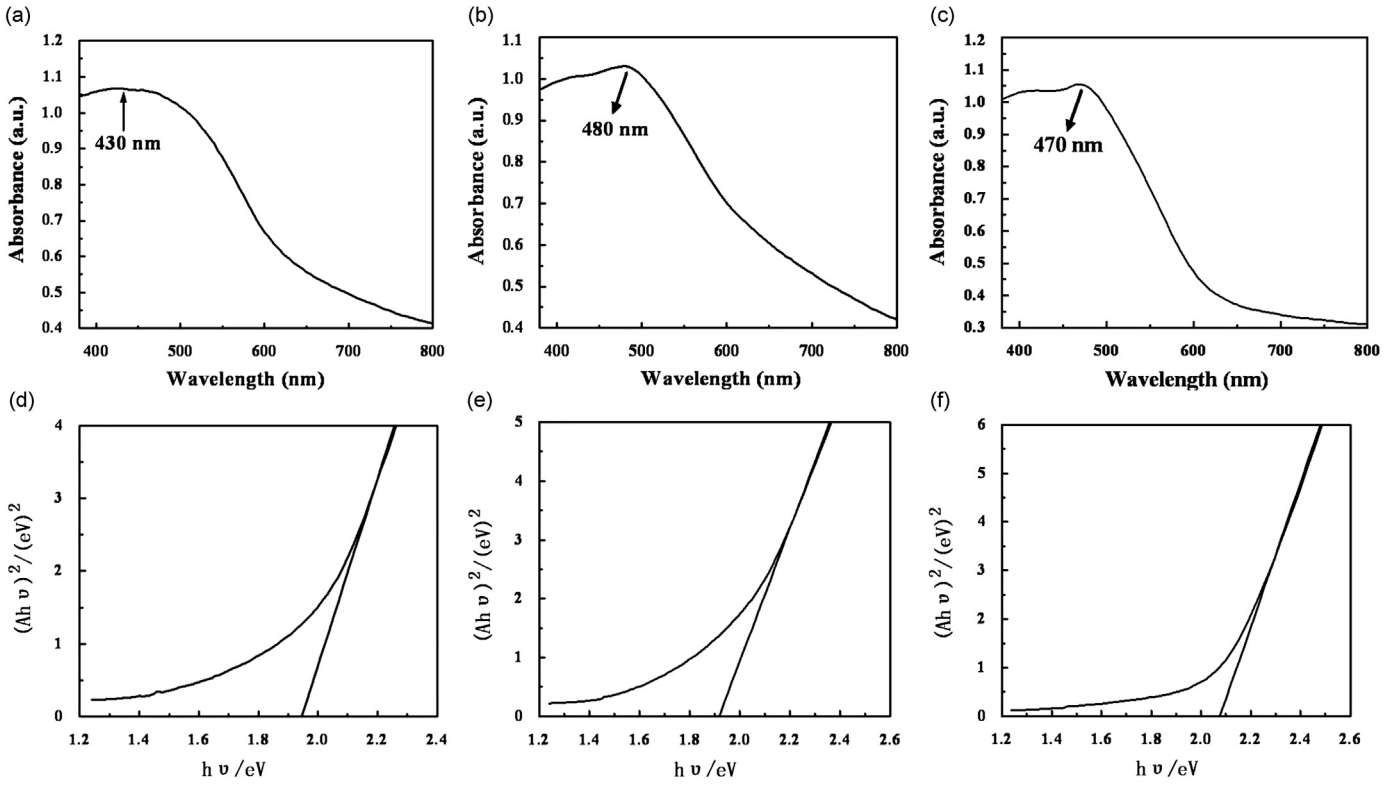

Fig. 9. UV–vis absorption spectra ((a), (c), (e)) and $(Ahv)^2$–hv curves ((b), (d), (f))of the Cu_2O samples ((a), (b) for truncated cube, (c), (d) for cuboctahedron, (e), (f) for octahedron).

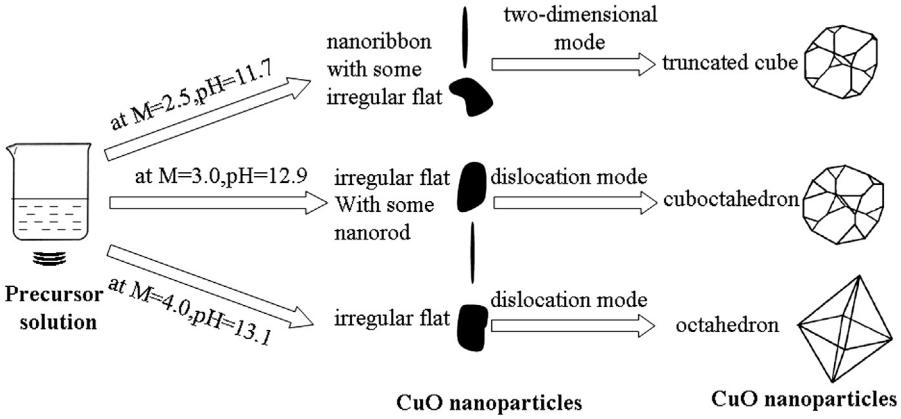

Fig. 10. The schematic illustration of the morphology evolution of cuprous oxide nanoparticles.

When appropriate ammonia is added to the aqueous solution of sodium hydroxide, the same precipitate is obtained after the aqueous solution of $CuSO_4 \cdot 5H_2O$ is mixed with them [Eq. (3)]. The CuO is also formed after the sonication reaction for 10 min [Eq. (4)], and is reduced to Cu_2O by ascorbic acid [Eq. (5)]. However, the excess ammonia can cause the precipitate dissolving, and the tetra ammine-copper (II) forms [Eq. (6)].

$$2CuO+C_6H_8O_6 \rightarrow Cu_2O+C_6H_6O_6+H_2O \quad (5)$$

$$Cu(H_2O)_4(OH)_2+4NH_3 \rightarrow [Cu(H_2O)_2(NH_3)_4]^{+}_{2}+2H_2O+2OH^{-} \quad (6)$$

As shown in Fig. 7, the formation rate of Cu^{2+} is a key factor when the ascorbic acid is excess in the process. Actually, the change of Cu^{+} supersaturation degree is the true reason of Cu_2O morphology variety [42]. According to the crystal theory, the morphology of nanocrystal depends on the relative growth rate of different crystal planes [43]. When the (111) plane grows relatively fast, the morphology of Cu_2O displays cube, when the (100) plane grows relatively fast, it displays octahedron [44]. In an aqueous solution system, the main growth modes of nanocrystal are the dislocation growth and the two-dimensional growth, which exists in a relatively high supersaturation system and an extremely low supersaturation system, respectively [45]. The (111) plane must grow via the two-dimensional mode [46]. So, different morphologies of Cu_2O can be obtained by controlling the formation rate of Cu^{2+}, which decides the Cu^{+} supersaturation degree. When $M=2.5$, the formation rate of Cu^{2+} is slow, resulting in the Cu^{+} supersaturation degree in the solution is also relatively low and situated at the two-dimensional mode. That is to say, that the (111) plane grows relatively fast, and the morphology of Cu_2O tends to be cube. At the same time, the excessive ascorbic acid corrodes the nanocube along (111) planes, and the H^{+} etches the area with high surface energy firstly, such as corners, to form the truncated Cu_2O nanocubes. With increasing the M value, the formation rate of Cu^{2+} accelerates and the Cu^{+} supersaturation degree in the solution rises. In this case, the dislocation mode becomes dominant, the (110) plane grows fast and the morphology of Cu_2O varies from truncated nanocube to cuboctahedron and further becomes octahedron. Fig. 10 shows the schematic illustration of the morphology evolution of cuprous oxide nanoparticles.

4. Conclusions

The cupric oxide (CuO) and cuprous oxide (Cu_2O) with various morphologies (i.e., nanospindle, nanorod, nanoribbon, and nano octahedron, etc.) were synthesized by a green sonochemical process without any surfactants and templates. The truncated cubic, cubic octahedral and octahedral Cu_2O nanoparticles could be prepared via the deoxidation of CuO nanoparticles. The optical properties of CuO and Cu_2O samples were affected considerably by the morphology. The growth mechanism of the CuO nanoparticles could be attributed to the sonohydrolysis-oriented aggregation-Ostwald ripening process. The morphology evolution of the cuprous oxide nanoparticles was due to the dislocation growth and two-dimensional growth modes. The experimental results indicate that the sodium hydroxide concentration has an impact on the morphology and size of CuO and Cu_2O nanoparticles synthesized.

Acknowledgments

This work was supported by the National Natural Science Foundation of China (No.50872034), Major Scientific and Technological Projects of Guangdong Province (No.2010A080405004), Project on the Integration of Industry, Education and Research of Guangdong Province (2012B091100451) and Applied Basic Research Program of Guangzhou (No.2012J4100006).

References

[1] L.S. Huang, S.G. Yang, T. Li, B.X. Gu, Y.W. Du, Y.N. Lu, S.Z. Shi, Preparation of large-scale cupric oxide nanowires by thermal evaporation method, Journal of Crystal Growth 260 (2004) 130–135.

[2] P. Gao, Y.J. Chen, H.J. Lv, X.F. Li, Y. Wang, Q. Zhang, Synthesis of CuO nanoribbon arrays with noticeable electrochemical hydrogen storage ability by a simple precursor dehydration at low temperature, International Journal of Hydrogen Energy 34 (2009) 3065–3069.

[3] S. Anandan, X.G. Wen, S.H. Yang, Room temperature growth of CuO nanorod arrays on copper and their application as a cathode in dye-sensitized solar cells, Materials Chemistry and Physics 93 (2005) 35–40.
[4] K.S. Jang, J.D. Kim, Facile and large-scale route to the fabrication of CuO nanosheets from a lamellar mesophase and their reversible self-assembly, Langmuir 25 (2009) 6028–6031.
[5] X.Q. Wang, G.C. Xi, S.L. Xiong, Y.K. Liu, B.J. Xi, W.C. Yu, Y.T. Qian, Solution-phase synthesis of single-crystal CuO nanoribbons and nanorings, Crystal Growth and Design 7 (2007) 930–934.
[6] X.Y. Song, H.Y. Yu, S.X. Sun, Single-crystalline CuO nanobelts fabricated by a convenient route, Journal of Colloid and Interface Science 289 (2005) 588–591.
[7] L.G. Yu, G.M Zhang, Y. Wu, X. Bai, D.Z. Guo, Cupric oxide nanoflowers synthesized with a simple solution route and their field emission, Journal of Crystal Growth 310 (2008) 3125–3130.
[8] Y.Y. Xu, D.R. Chen, X.L. Jiao, Fabrication of CuO pricky microspheres with tunable size by a simple solution route, Journal of Physical Chemistry B 109 (2005) 13561–13566.
[9] G. Jimenez-Cadena, E. Comini, M. Ferroni, G. Sberveglieri, Synthesis of Cu_2O bi-pyramids by reduction of $Cu(OH)_2$ in solution, Materials Letters 64 (2010) 469–471.
[10] C.H. Kuo, H.H. Michael, Fabrication of truncated rhombic dodecahedral Cu_2O nanocages and nanoframes by particle aggregation and acidic etching, Journal of the American Chemical Society 130 (2008) 12815–12820.
[11] F. Favier, E.C. Walter, M.P. Zach, T. Benter, R.M. Penner, Hydrogen sensors and switches from electrodeposited palladium mesowire arrays, Science 293 (2001) 2227–2231.
[12] H. Ahalapitiya Jayatissa, K. Guo, C. Ambalangodage Jayasuriya, Fabrication of cuprous and cupric oxide thin films by heat treatment, Applied Surface Science 255 (2009) 9474–9479.
[13] X.P. Gao, J.L. Bao, G.L. Pan, H.Y. Zhu, P.X. Huang, F. Wu, D.Y. Song, Preparation and electrochemical performance of polycrystalline and single crystalline CuO nanorods as anode materials for Li ion battery, Journal of Physical Chemistry B 108 (2004) 5547–5551.
[14] H.B. Wang, Q.M. Pan, J.W. Zhao, G.P. Yin, P.J. Zuo, Fabrication of CuO film with network-like architectures through solution-immersion and their application in lithium ion batteries, Journal of Power Sources 167 (2007) 206.
[15] L.Q. Lu, Y. Wang, Facile synthesis of graphene-supported shuttle-and urchin-like CuO for high and fast Li-ion storage, Electrochemistry Communications 14 (2012) 82–85.
[16] Y.J. Mu, J. Yang, S. Han, H.W. Hou, Y.T. Fan, Syntheses and gas-sensing properties of CuO nanostructures by using $[Cu(pbbt)Cl_2]_2 \cdot CH_3OH$ as a precursor, Materials Letters 64 (2010) 1287–1290.
[17] L. Li, Y.Y Zhan, Q. Zheng, Y.H. Zheng, X.Y. Lin, D.L. Li, J.J. Zhu, Water–gas shift reaction over aluminum promoted Cu/CeO_2 nanocatalysts characterized by XRD, BET, TPR and cyclic voltammetry (CV), Catalysis Letters 118 (2007) 91.
[18] Y.S. Chaudhary, A. Agrawal, R. Shrivastav, V.R. Satsangi, S. Dass, A study on the photoelectrochemical properties of copper oxide thin films, Intenational Journal of Hydrogen Energy 29 (2004) 131–134.
[19] K.H. Han, M. Tao, Electrochemically deposited p–n homojunction cuprous oxide solar cells, Solar Energy Materials and Solar Cells 93 (2009) 153–157.
[20] H.T. Zhu, J.X. Wang, G.Y. Xu, Fast synthesis of Cu_2O hollow microspheres and their application in DNA biosensor of hepatitis B virus, Crystal Growth and Design 9 (2009) 633–638.
[21] H.M. Yang, J. Ouyang, A.D. Tang, Y. Xiao, X.W. Li, X.D. Dong, Y.M. Yu, Electrochemical synthesis and photocatalytic property of cuprous oxide nanoparticles, Materials Research Bulletin 41 (2006) 1310–1318.
[22] W. Siripala, A. Ivanovskaya, T.F. Jaramillo, S.H. Baeck, E.W. McFarland, A Cu_2O/TiO_2 heterojunction thin film cathode for photoelectrocatalysis, Solar Energy Materials and Solar Cells 77 (2003) 229–237.
[23] H.M. Yang, J. Ouyang, A.D. Tang, Y. Xiao, X.W. Li, X.D. Dong, Y.M. Yu, Electrochemical synthesis and photocatalytic property of cuprous oxide nanoparticles, Materials Research Bulletin 41 (2006) 1310.
[24] B.J. Wood, H. Wise, R.S. Yolles, Selectivity and stoichiometry of copper oxide in propylene oxidation, Journal of Catalysis 15 (1969) 355–362.
[25] J.L. Li, L. Liu, Y. Yu, Y.W. Tang, H.L. Li, F.P. Du, Preparation of highly photocatalytic active nano-size TiO_2–Cu_2O particle composites with a novel electrochemical method, Electrochemistry Communications 6 (2004) 940.
[26] Q.W. Zhu, Y.H. Zhang, J.J. Wang, F.S. Zhou, P.K. Chu, Microwave synthesis of cuprous oxide micro-/nanocrystals with different morphologies and photocatalytic activities, Journal of Materials Science and Technology 27 (2011) 289–295.
[27] C.M. McShane, K.S. Choi, Photocurrent enhancement of n-Type Cu_2O electrodes achieved by controlling dendritic branching growth, Journal of the American Chemical Society 131 (2009) 2561–2569.
[28] N. Wang, Y. Cai, R.Q. Zhang, Growth of nanowires, Materials Science and Engineering R Reports 60 (2008) 1–51.
[29] Q. Liu, H.J. Liu, Y.Y. Liang, Z. Xu, G. Yin, Large-scale synthesis of single-crystalline CuO nanoplatelets by a hydrothermal process, Materials Research Bulletin 41 (2006) 697.
[30] Z.H. Yang, J. Xu, W.X. Zhang, A.P. Liu, S.P. Tang, Controlled synthesis of CuO nanostructures by a simple solution route, Journal of Solid State Chemistry 180 (2007) 1390.
[31] G. Sberveglieri, C. Baratto, E. Comini, G. Faglia, M. Ferroni, A. Ponzoni, A. Vomiero, Synthesis and characterization of semiconducting nanowires for gas sensing, Sensors and Actuators B Chemical 121 (2007) 208–213.
[32] C.H. Deng, H.M. Hu, W.L. Zhu, C.L. Han, G.Q. Shao, Green and facile synthesis of hierarchical cocoon shaped CuO hollow architectures, Materials Letters 65 (2011) 575–578.
[33] R. Vijaya Kumar, Y. Diamant, A. Gedanken, Sonochemical synthesis and characterization of nanometer-Size transition metal oxides from metal acetates, Chemistry of Materials 12 (2000) 2301.
[34] E.B. Flint, K.S. Suslick, The temperature of cavitation, Science 253 (1991) 1397–1399.
[35] K.S. Suslick, M.M. Fang, T. Hyeon, Sonochemical synthesis of iron colloids, Journal of the American Chemical Society 118 (1996) 1960.
[36] C.H. Deng, H.M. Hu, X.Q. Ge, C.L. Han, D.F. Zhao, G.Q. Shao, One-pot sonochemical fabrication of hierarchical hollow CuO submicrospheres, Ultrasonics Sonochemistry 18 (2011) 932–937.
[37] J.X. Xia, H. Li, Z.J. Luo, H. Shi, K. Wang, H.M. Shu, Y.S. Yan, Microwave-assisted synthesis of flower-like and leaf-like CuO nanostructures via room-temperature ionic liquids, Journal of Physics and Chemistry of Solids 70 (2009) 1461–1464.
[38] G.Q. Yuan, H.F. Jiang, C. Lin, S.J. Liao, Shape- and size-controlled electrochemical synthesis of cupric oxide nanocrystals, Journal of Crystal Growth 303 (2007) 400–406.
[39] V. Mayur, P. Angshuman, T. Sonal, Synthesis and characterization of cuprous oxide dendrites: new simplified green hydrothermal route, Journal of Alloys and Compounds 509 (2011) 523–528.
[40] M. Yang, J.J. Zhu, Spherical hollow assembly composed of Cu_2O nanoparticles, Crystal Growth 256 (2003) 134–138.
[41] C.H. Lu, M. Qi, Y.H. Wang, D.Y. Zhang, J.L. Xie, J.M. Ma, One-pot synthesis of octahedral Cu_2O nanocages via a catalytic solution route, Advanced Materials 17 (2005) 2562–2567.
[42] Y. Cao, Y.J. Wang, K.G. Zhou, Z. Bi, Morphology control of ultrafine cuprous oxide powder and its growth mechanism, Transactions of Nonferrous Metals Society of China 20 (2010) 216–220.
[43] J.B. Rawlings, S.M. Miller, W.R. Witkowski, Model identification and control solution crystallization processes: a review, Industrial and Engineering Chemistry Research 32 (1993) 1275–1296.
[44] H.F. Wu, Morphology and size control of silver oxide, silver and cuprous oxide micro-/nano-particles, Xiamen University (2007) 43–64.
[45] X.L. Yu, Present-day development of the mechanism research of crystal growth, Bulletin of National Science Foundation of China 16 (2002) 215–218.
[46] J.Y. Wang, Defect mechanism of crystal growth, Physics 30 (2001) 332–339.